



Contents lists available at ScienceDirect

Catalysis Today

journal homepage: www.elsevier.com/locate/cattod

Conversion of guaiacol over supported ReOx catalysts: Support and metal loading effect

K. Leiva^a, R. Garcia^a, C. Sepulveda^a, D. Laurenti^b, C. Geantet^b, M. Vrinat^b, J.L. Garcia-Fierro^c, N. Escalona^{d,e,f,*}

^a Universidad de Concepción, Facultad de Ciencias Químicas, Casilla 160C, Concepción, Chile

^b IRCELYON, UMR 5256 CNRS, Université Lyon 1, 2 Avenue A. Einstein, 69626 Villeurbanne Cedex, France

^c Instituto de Catálisis y Petroquímica, CSIC, Cantoblanco, 28049 Madrid, Spain

^d Departamento de Ingeniería Química y Bioprocesos, Escuela de Ingeniería, Pontificia Universidad Católica de Chile, Avenida Vicuña Mackenna 4860, Macul, Santiago, Chile

^e Departamento de Química Física, Facultad de Ciencias Químicas, Pontificia Universidad Católica de Chile, Chile

^f Centro de Investigación en Nanotecnología y Materiales Avanzados (CIEN-UC), Pontificia Universidad Católica de Chile, Santiago, Chile

ARTICLE INFO

Keywords:

Guaiacol
Supported
ReOx
Biomass
HDO

ABSTRACT

In the present work, the catalytic activity and selectivity for the conversion of 2-methoxyphenol over ReOx catalysts supported on SiO₂, Al₂O₃ and SiO₂-Al₂O₃ in a batch reactor at 300 °C and 5 MPa of hydrogen pressure were studied. Additionally, several SiO₂-supported ReOx catalysts were synthesized with different metal loadings. These catalysts were characterized by N₂ adsorption, X-ray photoelectron spectroscopy (XPS), temperature programmed reduction (TPR), temperature-programmed desorption of ammonia (TPD-NH₃), Raman spectroscopy and ultraviolet visible (UV-vis-DR) spectroscopy. ReOx catalyst supported over SiO₂ revealed the highest catalytic activity and selectivity towards deoxygenated products. This was attributed to a higher formation of oxygen vacancies (active sites) on SiO₂, due to a weaker metal-support interaction. The increase of Re content on SiO₂ resulted in an increase of guaiacol conversion, reaching a maximum at about 1.8 atoms of Re per nm² of support. The decrease of activity over 1.8 atoms of Re per nm² of support was correlated to loss of active site due to the formation of aggregates of ReOx.

1. Introduction

The increase in worldwide energy demand, the decrease of fossil fuel reserves and the negative environmental impact of fossil fuel have led to focus on renewable and sustainable carbon sources. In this context, lignocellulosic biomass is one of the main attractive alternatives to fossil fuels as this kind of biomass is available in many countries and does not compete with food production.

Different thermochemical conversion processes can be employed to convert biomass to chemicals and fuels [1]. For example, through fast pyrolysis (400–500 °C under inert atmosphere), bio-oil is produced at relatively high yields (60%), and this liquid is a potential source of biofuels and chemicals [2,3]. However, the pyrolytic bio-oil cannot be directly used as fuel due to their high viscosity, corrosiveness and thermal instability making it impossible for storage and transport. This is due to complex mixture of oxygen-containing compounds in the form of phenol derivatives, aldehydes, ketones, carboxylic acids, esters and

aliphatic alcohols in bio-oil [4–7]. To upgrade bio-oil, a catalytic hydrotreating method known as hydrodeoxygenation (HDO) can be utilized to remove oxygen in the form of H₂O to improve the fuel properties of bio-oil [8,9]. Because of the complexity of the composition of bio-oil, the high amount of water and the presence of lignin fragments, investigations dealing with bio-oil upgrading are focused mainly on highly representative compounds. In this context, guaiacol (2-methoxyphenol) which is representative of the lignin units in bio-oil has become an attractive molecule for HDO studies [10–14].

To perform catalytic hydrodeoxygenation reactions, sulfides [13,15–17], nitrides [18–20], and noble and non-noble metal based catalysts [21–23] are the most commonly studied active phases. The principal disadvantage of sulfide catalysts is the necessity of external addition of a sulfiding agent to keep the sulfide phase. Thus, there has been a recent shift on exploring non-sulfide catalysts for HDO. In this context, it has been reported that reduced metallic catalysts displayed higher activity and selectivity to hydrodeoxygenated compounds than

* Corresponding author at: Departamento de Ingeniería Química y Bioprocesos, Escuela de Ingeniería, Pontificia Universidad Católica de Chile, Avenida Vicuña Mackenna 4860, Macul, Santiago, Chile.

E-mail address: neescalona@ing.puc.cl (N. Escalona).

<http://dx.doi.org/10.1016/j.cattod.2017.04.002>

Received 5 February 2017; Received in revised form 21 March 2017; Accepted 4 April 2017
0920-5861/ © 2017 Elsevier B.V. All rights reserved.

conventional sulfide catalysts [24].

Transition metal carbides, nitrides and phosphides have also shown promise in HDO. Boullouso-Eiras et al. [25] compared the catalytic activity of TiO₂-supported Mo carbide, nitride, phosphide and oxide catalysts in phenol HDO reaction, and showed that MoO₃ catalyst displayed the highest activity. However, all the catalysts presented similar selectivity to benzene and cyclohexene.

Shetty et al. [26] studied the HDO of *m*-cresol to toluene on supported molybdenum oxide catalysts at very low H₂ pressure (≤ 1 bar). The authors found that catalysts supported on TiO₂ and ZrO₂ were highly active and stable due to stabilization of MoO₃ oxidation states. Moreover, the authors proposed that the activity of Mo oxide is related to coordinatively unsaturated Mo sites (oxygen vacancies).

Rhenium is one of the non-conventional catalysts that have been extensively used in hydrotreating reactions, in both sulfide and metallic phases [13,14,17,27–32]. Initial efforts were focused on ReS₂ as an active phase in hydrodesulfurization [17,29,30,33], and HDO reactions [13,14,17,28], in which ReS₂/SiO₂ catalyst presented a higher activity than conventional NiMoS/Al₂O₃ catalyst. This behavior was attributed to metal-like character of ReS₂ which favored hydrogenation [31].

Previously, we studied the hydrodeoxygenation of guaiacol over silica-supported Re oxide, Re metal, and Re sulfide catalysts [34]. The highest activity was obtained on ReOx/SiO₂ catalyst; furthermore, this catalyst was highly selective towards benzene and cyclohexane. In contrast, ReS₂/SiO₂ and Re/SiO₂ catalysts principally produced phenol. The unique behavior of ReOx/SiO₂ was attributed to the presence of oxygen vacancies.

In order to further improve the performance of ReO_x catalysts, it is important to understand some fundamental factors that control reactivity, such as the influence of support and metal loading. These properties are yet to be studied for ReO_x catalysts for HDO reactions. Therefore, the objective of this work is to understand the effect of support and metal content on the conversion of guaiacol as a lignin model molecule. This was achieved by comparison of the reactivity of well-characterized ReOx supported on SiO₂, Al₂O₃ and SiO₂-Al₂O₃ catalysts in the HDO of guaiacol at 300 °C and 5 MPa of hydrogen pressure in a batch reactor. The effect of metal content was carried out using the most active catalytic system.

2. Experimental

2.1. Catalyst preparation

The catalysts were prepared by incipient wetness impregnation with aqueous solution of NH₄ReO₄ (Aldrich, 99%) on different supports (Silica Grace 432, Al₂O₃ SPH 501, and SiO₂-Al₂O₃ Ketjen HA 100 SP (26.2% Al₂O₃)). For the study of the support effect, the catalysts were prepared with a Re nominal loading of 1.8 atoms of Re per nm² of support. The impregnated catalysts were left for maturation at room temperature for 24 h, dried at 120 °C for 12 h and then calcined at 300 °C for 0.5 h. For the study of the effect of metal loading, the catalysts were prepared with a loading of 0.6–2.7 atoms of Re per nm² of SiO₂ support following the previously described procedure. The Re content was determined by ICP using the line of emission 221.426 nm of Re. The values are summarized in Table 1.

2.2. Characterization of the supports and catalysts

The BET surface area (S_{BET}) and the total pore volume (V_p) of catalysts and supports were determined from nitrogen adsorption-desorption isotherms at -196 °C using a Micromeritics-TriStar II 3020 instrument.

Temperature programmed reduction (TPR) studies were carried out in a quartz cell on a conventional system equipped with a thermal conductivity detector. In each experiment, 100 mg of the sample was

heated in 5% H₂/Ar mixture under 50 cm³ min⁻¹ flow. The samples were heated from 25 °C to 1050 °C with a heating rate of 10 °C min⁻¹.

XPS measurements were performed using a VG Escalab 200R electron spectrometer equipped with a hemispherical electron analyzer and Mg K α (1253.6 eV) excitation source. Energy corrections were performed using the line of each support as internal reference. The intensity of the peaks was estimated by calculating the integral of each peak after subtracting an S-shaped background and fitting the experimental curve to a combination of Gaussian/Lorentzian lines.

The UV-vis-DR spectra of dried samples were measured using a UV-vis-Lambda 35 PerkinElmer Spectrophotometer, equipped with a quartz cell, provided with a diffuse reflectance sphere for powder analysis (Labsphere). Before analysis, all samples were milled using an agate mortar and diluted with BaSO₄ to maximize reflectance. The UV-vis-DR spectra were recorded in the wavelength range 200–1100 nm at ambient conditions. The spectra obtained were decomposed with the PeakFit v4.12 software.

Raman spectra of the supported metal oxide catalysts were collected from 0 to 3000 cm⁻¹ with a LabRam HM Raman spectrometer (Horiba-JobinYvon) equipped with a BXM confocal microscope, employing the 514.5 nm line of an Ar⁺ laser as the excitation source. All the recorded data were treated using the LABSPEC software.

Temperature-programmed desorption of ammonia (TPD-NH₃) analyses were performed in a TPR/TPD Micromeritics 2900 system equipped with a thermal conductivity detector (TCD). Prior to analysis the samples were cleaned under He flow of 50 mL min⁻¹ at 383 K for 30 min, and then subjected to ammonia pulses until saturation of the catalyst surface at 120 °C. Then, the samples were cooled to room temperature under He, followed by flushing under He to remove weakly adsorbed NH₃. Once the baseline was stabilized, TPD-NH₃ measurements were performed while the temperature was increased linearly to 700 °C with a heating rate of 10 °C min⁻¹.

2.3. Catalytic tests

The conversion of guaiacol was carried out in an autoclave reactor operating in batch mode. The liquid reactant feed, consisting of guaiacol (0.232 mol L⁻¹) in *n*-dodecane (80 mL) with hexadecane (0.0341 mol L⁻¹) as an internal standard, were introduced into the reactor together with 0.200 g of solid catalyst. The system was closed, and N₂ was bubbled through the solution for 10 min with a 100 mL min⁻¹ flow to purge the system. The reactor was heated under stirring to the reaction temperature of 300 °C under N₂ atmosphere. The initial reaction time (t_0) was defined when the reaction temperature was reached and the pressure was adjusted to 5 MPa of H₂. The pressure was kept constant during the course of the experiment. Liquid samples were taken periodically during the reaction (0, 10, 15, 30, 60, 120, 180, 240 and 300 min), and were analyzed by gas chromatography (Perkin-Elmer Clarus 680) GCMS-SQ8T, and quantified by gas chromatography (Perkin-Elmer Clarus 400) equipped with a Flame Ionization Detector (FID) and a CP-Sil 5 column (Agilent, 30 m \times 0.53 mm \times 1.0 μ m film thickness). The specific rate for the total conversion of guaiacol was calculated from the initial slope of conversion as a function of time plot according to the following equation:

$$r_s = \frac{[b \times n]}{m} \quad (1)$$

Where r_s is the specific rate (moles of guaiacol transformed per gram of catalyst per second and expressed in mol. g_{cat}⁻¹s⁻¹), b represents the initial slope of the conversion vs. time plot (s⁻¹), n is the initial moles of guaiacol (mol), and m is the mass of catalyst (g). The intrinsic rate was calculated from the specific rate according to the following equation:

$$r_i = \frac{r_s}{n_{\text{Re}}} \times N_{\text{av}} \quad (2)$$

Where r_i is the intrinsic rate (i.e. molecules of guaiacol transformed per

Table 1
Textural properties of supports and catalysts.

Samples	Re ₂ O ₇ content (%)	Re surface density (atoms nm ⁻²)	S _{BET} (m ² g ⁻¹)	V _p (cm ³ g ⁻¹)	V _o (cm ³ g ⁻¹)	V _m (cm ³ g ⁻¹)
SiO ₂	–	–	305	1.1	0.20	0.90
SiO ₂ -Al ₂ O ₃	–	–	352	0.60	0.20	0.40
γ-Al ₂ O ₃	–	–	240	0.50	0.14	0.36
ReOx(1.8)/SiO ₂ -Al ₂ O ₃	13	1.8	214	0.40	0.15	0.25
ReOx(1.8)/γ-Al ₂ O ₃	15	1.8	171	0.30	0.10	0.20
ReOx(0.6)/SiO ₂	6	0.6	306	1.03	0.14	0.89
ReOx(1.3)/SiO ₂	11	1.3	281	0.88	0.13	0.75
ReOx(1.8)/SiO ₂	14	1.8	265	0.88	0.12	0.67
ReOx(2.2)/SiO ₂	17	2.2	236	0.72	0.11	0.61
ReOx(2.7)/SiO ₂	21	2.7	224	0.68	0.10	0.58

Re atoms per second and expressed in molec. Re at⁻¹s⁻¹), n_{Re} is the number of Re atoms per gram of catalyst, and N_{AV} is the Avogadro's number.

The selectivities (%) were determined at 20% and 50% of guaiacol conversion, according to the following equation:

$$S\% = \frac{X_i}{X_T} \times 100 \quad (3)$$

Where X_i is the percentage of product I formed, and X_T is the guaiacol conversion.

3. Results and discussion

3.1. Support effect

The BET surface areas (S_{BET}), micropore (V_o), mesopore (V_m) and total (V_p) pore volumes of the supports and catalysts are summarized in Table 1. It can be noted that the surface area of the supports varied in the order SiO₂-Al₂O₃ > SiO₂ > γ-Al₂O₃. Also, it shows that the S_{BET} and pore volumes of the three catalysts with the same Re content (1.8 atoms of Re per nm² of support) decreased in comparison with the corresponding supports; more specifically, a decrease in the S_{BET} of 13% for SiO₂, 39% of SiO₂-Al₂O₃ and 29% for Al₂O₃. These results suggest that ReO₄⁻ species were best dispersed on silica where it is observed that the micropore and mesopore volume decrease only slightly after impregnation, indicating that blockage of the mouth of the pores is virtually absent. Meanwhile, the highest decrease of S_{BET} observed for ReOx(1.8)/SiO₂-Al₂O₃ in comparison with SiO₂-Al₂O₃ support suggests a partial blocking at the mouth of the pores.

Fig. 1a shows the TPR profiles of ReOx(1.8)/support catalysts. It can be seen that the ReOx(1.8)/SiO₂ catalyst presented a single reduction peak at 341 °C. This suggests a single reduction step of ReOx species to metallic Re on silica, in agreement with the results of Arnoldy et al. [35]. However, the TPR profile of ReOx(1.8)/γ-Al₂O₃ displayed two reduction peaks centered at 361 °C and 383 °C. Similarly, the ReOx(1.8)/SiO₂-Al₂O₃ catalysts displayed two reduction peaks, but they were centered at 363 °C and 378 °C. The inset of Fig. 1a shows that reduction of NH₄ReO₄ precursor occurs at 387 °C, while that of bulk ReO_x (obtained after calcinations of NH₄ReO₄ at 300 °C for 0.5 h) occurs at a lower temperature of 358 °C. Therefore, the low-temperature peak observed for ReOx(1.8)/γ-Al₂O₃ and ReOx(1.8)/SiO₂-Al₂O₃ can be attributed to ammonium perrhenate species, which were not completely decomposed during calcination, in accordance with previous observations made by Arnoldy et al. [35]. On the other hand, the higher-temperature peak could be assigned to rhenium oxide species present on the surface of the catalyst. The difference in behavior between the SiO₂-supported catalyst and the other supported catalysts can be attributed to different acid-base properties of each support, affecting the strength of the interaction between ReOx or ReO₄⁻ species and the surface of the supports. Another notable observation from Fig. 1a is the difference in intensity of the reduction peaks (particularly the higher-

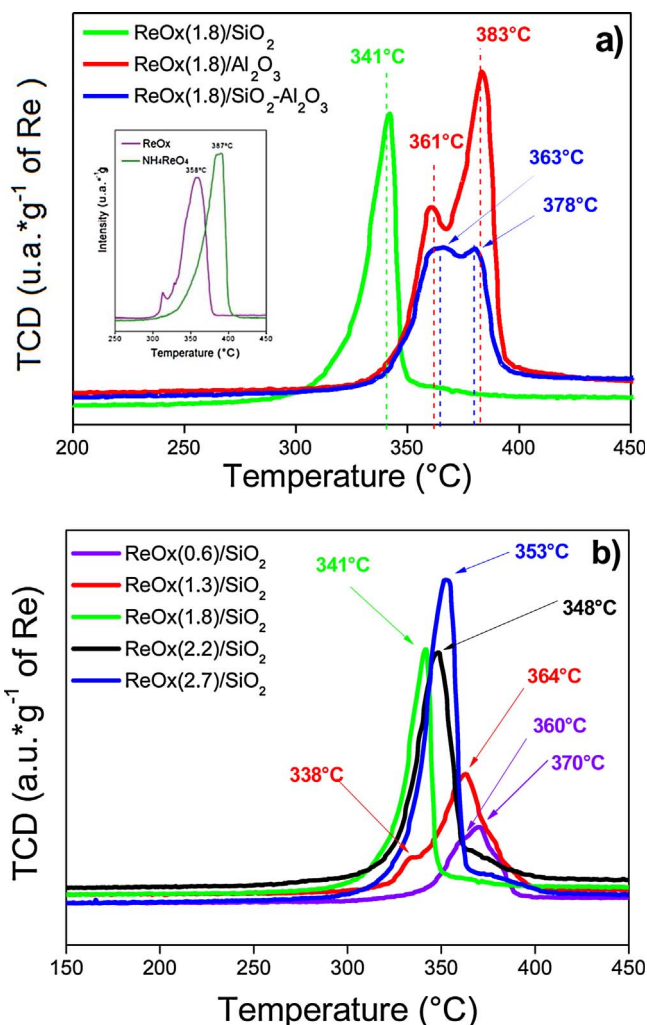


Fig. 1. TPR profiles of a) ReOx(1.8)/support and b) ReOx(x)/SiO₂ catalysts. Inset Fig. 1a: TPR of NH₄ReO₄ and ReOx (after calcination of NH₄ReO₄ for 0.5 h at 300 °C).

temperature peak) of ReOx(1.8)/SiO₂-Al₂O₃ and ReOx(1.8)/γ-Al₂O₃ despite the nearly identical reduction temperatures. This is because the catalysts were prepared with identical Re surface density but contain different metal loadings (in wt%) due to the different S_{BET} of the supports. Furthermore, Arnoldy et al. [35] studied the reduction temperature of Re₂O₇ catalysts supported on Al₂O₃, SiO₂ and carbon, and found that the difference in reducibility was due to a variation in the strength and heterogeneity of the Re⁷⁺-support interaction, which depended on the support used, and decreased in the order, Al₂O₃ > SiO₂ > carbon. Mitra et al. [36] found that the reduction temperature of ReOx species correlated with the binding energy

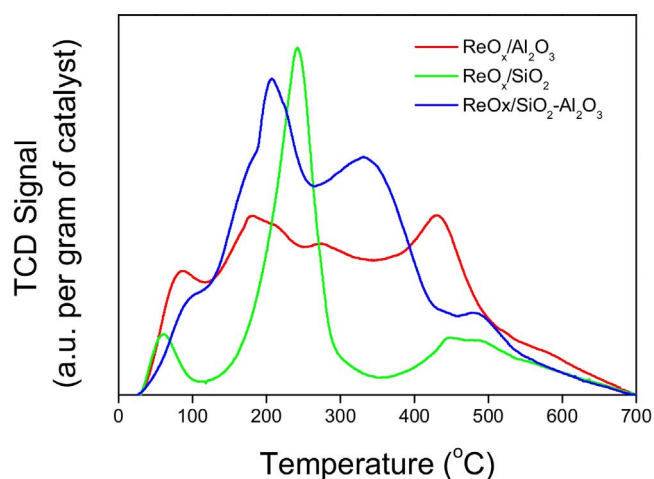


Fig. 2. Temperature-programmed desorption of ammonia (TPD-NH₃) for ReO_x(1.8)/SiO₂, ReO_x(1.8)/Al₂O₃ and ReO_x(1.8)/SiO₂-Al₂O₃ catalysts.

Table 2

Surface acid sites calculated from NH₃ desorption (TPD-NH₃).

Catalysts	Weak acid sites (10 ⁻⁴ mol NH ₃ g ⁻¹)	Medium acid sites (10 ⁻⁴ mol NH ₃ g ⁻¹)	Strong acid sites (10 ⁻⁴ mol NH ₃ g ⁻¹)	Total acid sites (10 ⁻⁴ mol NH ₃ g ⁻¹)
ReO _x (1.8)/ SiO ₂ - Al ₂ O ₃	1.14	1.41	0.29	3.17
ReO _x (1.8)/ Al ₂ O ₃	1.59	0.31	0.78	2.68
ReO _x (1.8)/ SiO ₂	0.95	0.17	0.14	1.26

between the metal and the support, which decreased in the following order: Re-O-Al > Re-O-Si-Al > Re-O-Si. Therefore, these results suggest that less acidic supports like SiO₂ promote a weak interaction with the ReO_x or NH₄ReO₄ species, favoring only one low-temperature reduction peak. Meanwhile, the acid sites present on the γ -Al₂O₃ and SiO₂-Al₂O₃ supports could favor a stronger interaction with ReO₄⁻ and ReO_x

Table 3

XPS binding energies (eV) and surface atomic ratios of Si2p, Al2p, O1s and Re4f species for the oxides catalysts.

Catalysts	Si2p (eV.)	Al2p (eV.)	O1s (eV.)	Re4f (eV.)	Re/M (Si, Al, Si + Al) at
ReO _x (1.8)/Al ₂ O ₃	-	74.5	532.7	46.3	0.073
ReO _x (1.8)/SiO ₂ - Al ₂ O ₃	103.4	75.2	532.8	46.2	0.153
ReO _x (0.6)/SiO ₂	103.4	-	532.8	46.1 (65) 47.3 (35)	0.022
ReO _x (1.3)/SiO ₂	103.4	-	532.8	45.9 (55) 47.5 (45)	0.040
ReO _x (1.8)/SiO ₂	103.4	-	532.7	45.9 (53) 47.5 (47)	0.054
ReO _x (2.2)/SiO ₂	103.4	-	532.7	45.7 (63) 47.4 (37)	0.041
ReO _x (2.7)/SiO ₂	103.4	-	532.7	45.6 (59) 47.3 (41)	0.042

species, shifting their reduction peak to higher temperature.

Fig. 2 presents the temperature-programmed desorption of ammonia (TPD-NH₃) of ReO_x(1.8)/SiO₂, ReO_x(1.8)/Al₂O₃ and ReO_x(1.8)/SiO₂-Al₂O₃ catalysts. The strength of the acid sites of the catalysts are related to the temperature of NH₃ desorption: weak acid sites (< 300 °C), medium acid sites (between 300 °C and 500 °C), and strong acid sites (> 500 °C)[37]. According to this classification, Fig. 2 shows that all the three catalysts possess weak and medium acid sites, but with different peak intensities, indicating an influence of the support. Table 2 presents the acid site distribution and the total acid sites expressed as quantity of ammonia desorbed per gram of catalyst. The ReO_x(1.8)/Al₂O₃ and ReO_x(1.8)/SiO₂ catalysts presented a predominance of weak acid sites, while ReO_x(1.8)/SiO₂-Al₂O₃ displayed the highest amount of medium acid sites. The total acid sites decreased in order: ReO_x(1.8)/SiO₂-Al₂O₃ > ReO_x(1.8)/Al₂O₃ > ReO_x(1.8)/SiO₂ catalysts. However, it must be pointed out that ReO_x(1.8)/Al₂O₃ had the highest number of strong acid sites.

XPS spectra of Re 4f region of ReO_x(1.8)/SiO₂, ReO_x(1.8)/Al₂O₃ and ReO_x/SiO₂-Al₂O₃ catalysts are shown in Fig. 3. Curve fitting of the spectra for ReO_x(1.8)/SiO₂ revealed two partially overlapped doublet, each one containing the Re 4f_{7/2} and 4f_{5/2} peaks. Meanwhile, curve fitting of the spectra of ReO_x(1.8)/Al₂O₃ and ReO_x/SiO₂-Al₂O₃ cata-

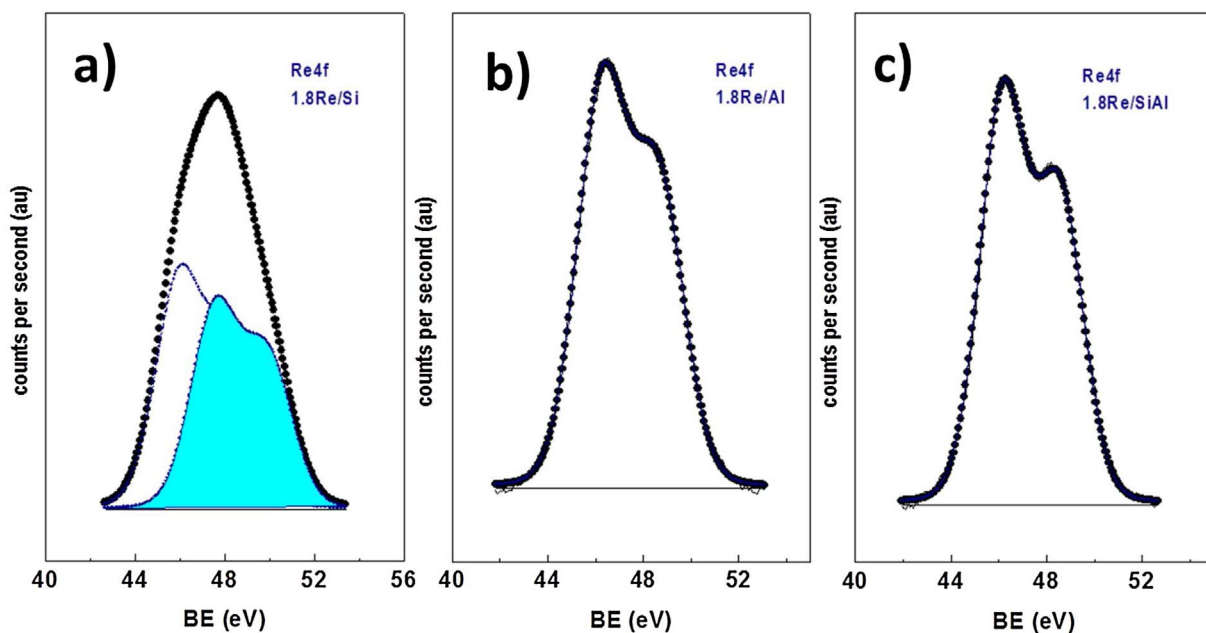


Fig. 3. X-ray photoelectron spectra of the Re 4f region on: a) ReO_x(1.8)/SiO₂, b) ReO_x(1.8)/Al₂O₃ and c) ReO_x(1.8)/SiO₂-Al₂O₃ catalysts.

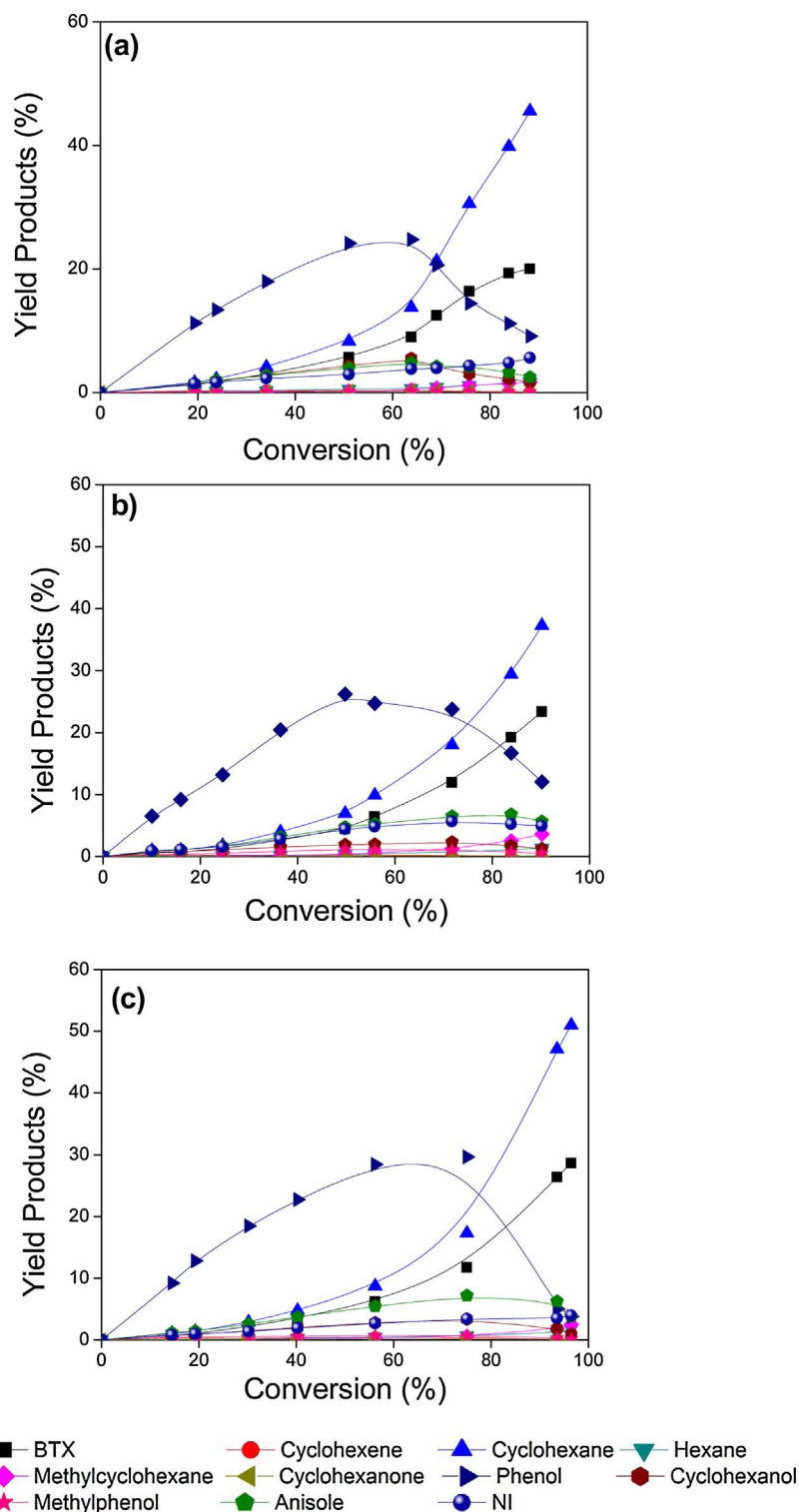


Fig. 7. Yield of product in function of guaiacol conversion of a) $\text{ReOx}(1.8)/\text{SiO}_2$, b) $\text{ReOx}(1.8)/\text{Al}_2\text{O}_3$ and c) $\text{ReOx}(1.8)/\text{SiO}_2\text{-Al}_2\text{O}_3$ catalyst.

In order to identify the different ReO_x species on SiO_2 support, the $\text{ReO}_x(x)/\text{SiO}_2$ catalysts were characterized by Raman spectroscopy and their spectra are shown in Fig. 4. The spectrum of NH_4ReO_4 , included in this figure as a reference, shows 4 characteristic bands centered at 342, 891, 914 and 965 cm^{-1} . The bands centered at 342 and 965 cm^{-1} are attributed to symmetric stretching of the terminal $\text{Re}=\text{O}$ bonds of ReO_4^- surface species [36,44–47]. Meanwhile, the band centered at 891 cm^{-1} corresponds to $\text{Re}-\text{O}-\text{Re}$ bond vibration [36,44–47].

The four $\text{ReO}_x/\text{SiO}_2$ catalysts (Fig. 4) present the same four char-

acteristic bands of solid perrhenate (used as precursor). However for $\text{ReO}_x(1.3)/\text{SiO}_2$, the peaks are not intense and we had to use a lower range to get a spectrum. This figure also shows that from 1.8 atoms of Re per nm^2 of support, a new Raman band centered at 990 cm^{-1} appears. This band has also been assigned to tetrahedral ReO_4^- surface species [36,44,45], and suggests the formation of larger ReO_4^- crystals.

Fig. 5 depicts the UV–vis–DR spectra of the $\text{ReO}_x(x)/\text{SiO}_2$ catalysts. The catalysts containing 0.6 atoms of Re per nm^2 exhibited a very

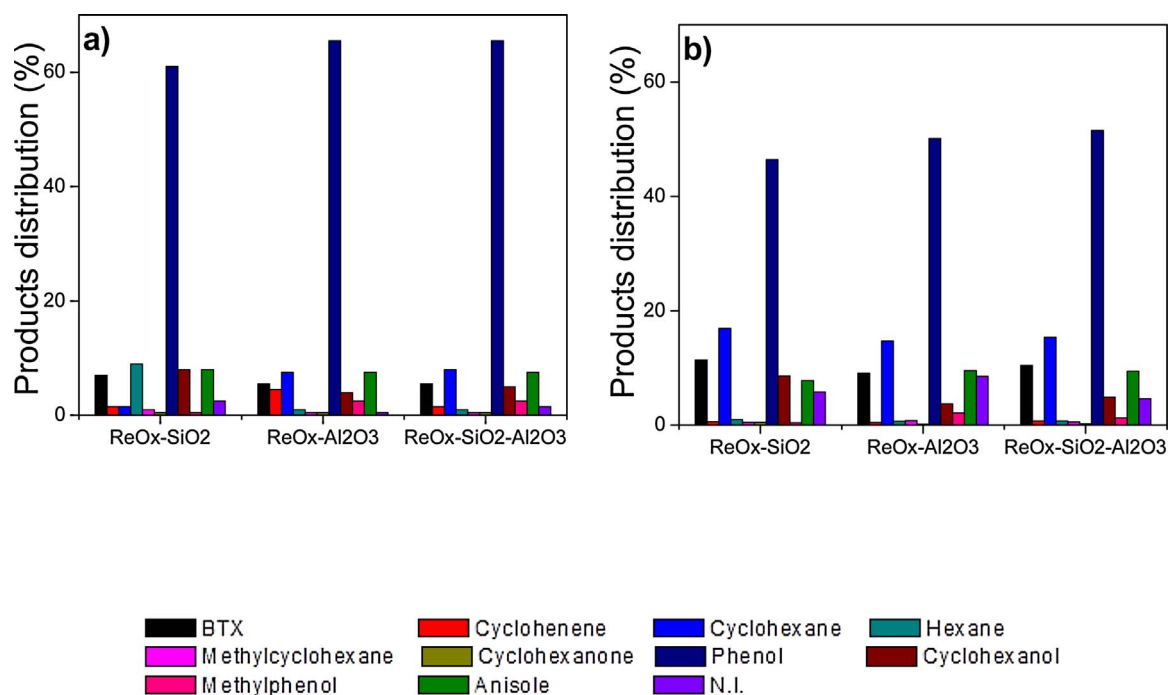


Fig. 9. Products distribution on ReOx(1.8)/support catalysts calculated at a) 20% and b) 50% of guaiacol conversion.

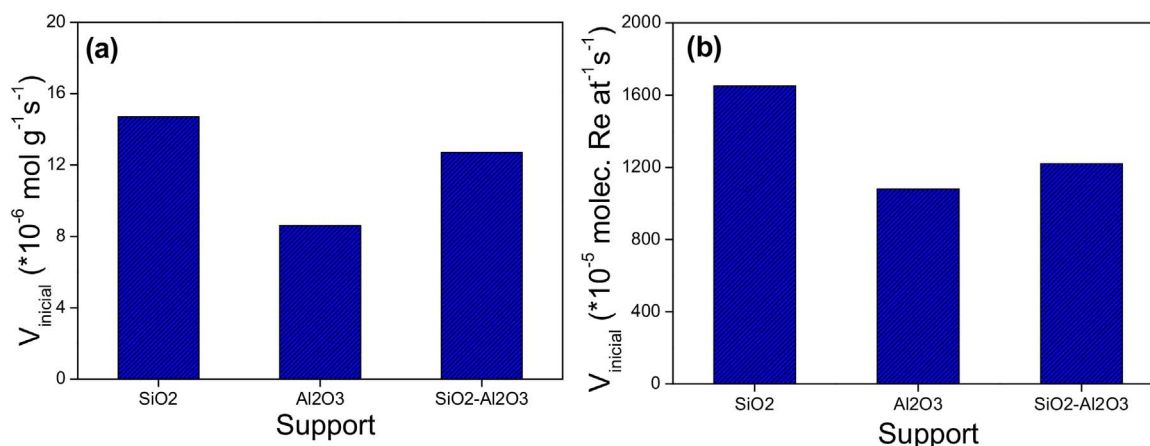


Fig. 10. a) Initial specific rates and b) intrinsic rates over ReOx(1.8)/support catalysts.

toluene, traces of xylene) and cyclohexane. As side products, the formation of cyclohexanol and anisole were observed. The formation of methanol, cyclohexene, hexane, methylcyclohexane, cyclohexanone and methyl phenol were also observed but the total yield of these products were very small (< 2%). Phenol and anisole production increased with time and then decreased, indicating that both compounds are intermediate products. Thus, these results are consistent with the guaiacol conversion scheme previously reported by Leiva et al. [34] for ReOx/SiO₂ catalyst, which was adapted from Laurent and Delmon [50], Bui et al. [15,51] and Nimmanwudipong et al. [52], and shown in Fig. 8. On the basis of this reaction scheme, guaiacol can be transformed by direct deoxygenation route (DDO) to form anisole, by direct demethoxylation (DMO) to form phenol, by demethylation (DME) to form catechol (it was not detected) and by hydrogenation (HYD) to form methoxycyclohexanone. Then, benzene can be formed by DDO of phenol or by DMO of anisole. Cyclohexene can be formed by HYD of benzene or DMO of methoxycyclohexanone to form cyclohexanone, followed by hydrogenation and dehydration. On the other hand, methylation (ME) of phenol to methylphenol can occur, followed by DDO to toluene. Xylene (detected in trace amount) can be formed either

by successive methylation of phenols and DDO or by ME of toluene. Meanwhile, methylcyclohexane can be formed by HYD of toluene or methylcyclohexene. Finally, cyclohexane (traces) could form hexane through the cracking route (CR). These results show that ReOx/support catalysts have a high potential for the hydrogenolysis of C–OH bond. The products distribution calculated at 20% and 50% of guaiacol conversion over the catalysts dispersed on different supports (ReOx(1.8)/supports) is shown in Fig. 9. The catalysts displayed similar products of reaction with phenol as the main product. However, methylphenol was only observed with the ReOx(1.8)/SiO₂-Al₂O₃ and ReOx(1.8)/Al₂O₃ catalysts. Since this product is formed via a methylation step which is promoted in the presence of acid sites, this result is consistent with TPD-NH₃ results which shows these two catalysts to be the most acidic catalysts, and agrees with the findings of Bui et al. [15,51]. It should be pointed out that unlike studies over other active phases, such as CoMo sulfide [51], metallic Ni [53], metal nitrides [19], among others, which have shown a strong dependence of products distribution on the surface properties of the support, ReOx species appear to have a stronger influence on the reaction pathway than the support. This result further highlights the unique abilities of ReOx

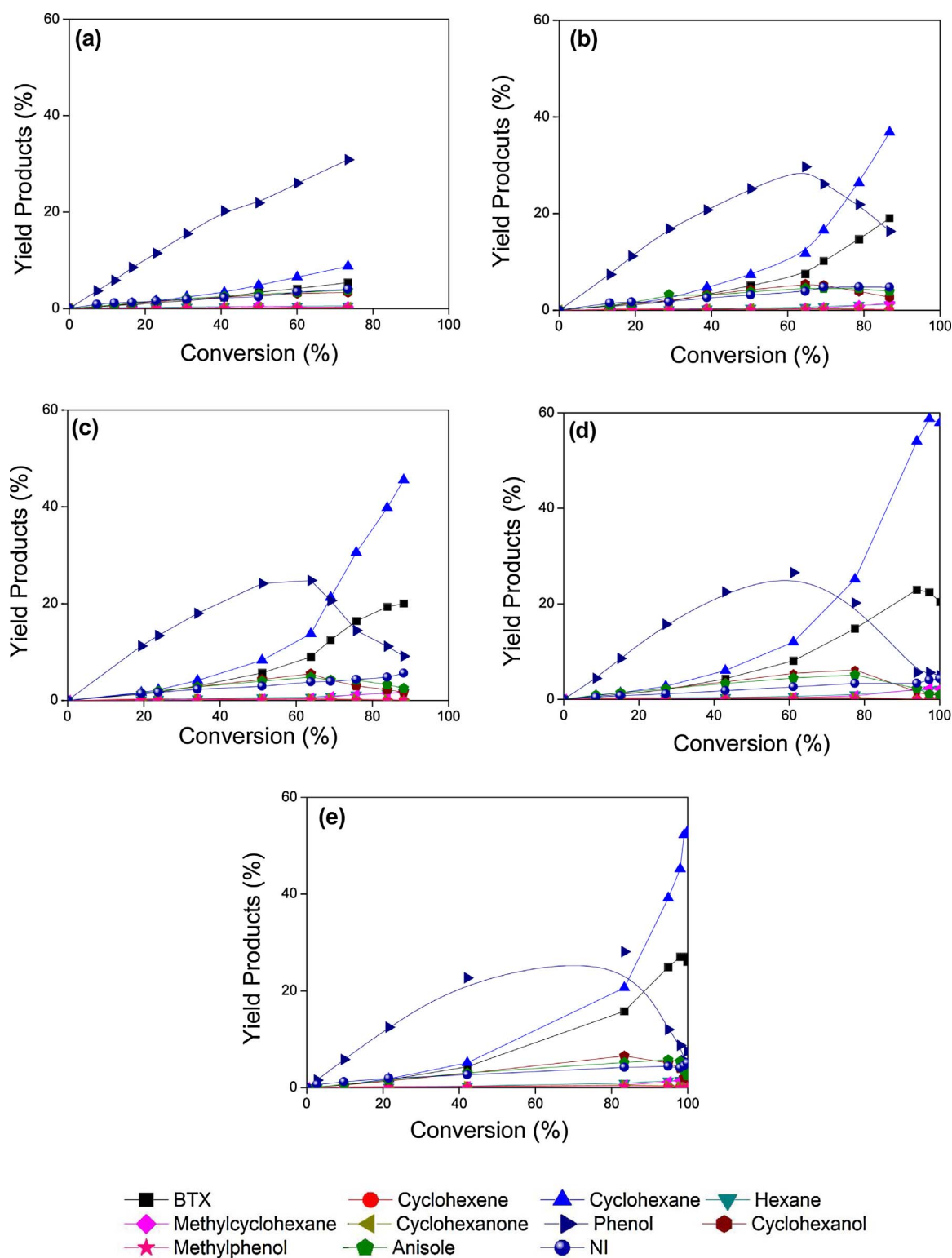


Fig. 11. Yield of products as a function of guaiacol conversion over a) $\text{ReOx}(0.6)/\text{SiO}_2$, b) $\text{ReOx}(1.3)/\text{SiO}_2$, c) $\text{ReOx}(1.8)/\text{SiO}_2$, d) $\text{ReOx}(2.2)/\text{SiO}_2$ and e) $\text{ReOx}(2.7)/\text{SiO}_2$ catalysts.

catalysts in HDO reactions.

The specific (per mass of catalyst) and intrinsic (per Re atoms) catalytic activities for the $\text{ReOx}(1.8)/\text{support}$ catalysts are depicted in Fig. 10. Fig. 10a and 10b show $\text{ReOx}(1.8)/\text{SiO}_2$ to be the most active catalyst, followed by $\text{ReOx}(1.8)/\text{SiO}_2\text{-Al}_2\text{O}_3$ and $\text{ReOx}(1.8)/\text{Al}_2\text{O}_3$ catalysts. This trend cannot entirely be related to the relative Re dispersion obtained from XPS results. In fact, XPS results show that the most active catalyst, $\text{ReOx}(1.8)/\text{SiO}_2$, displayed the lowest Re/Si

(Al, Si + Al) atomic ratio. On the other hand, TPR results showed that Re oxides were reduced at a lower temperature on the SiO_2 support than over Al_2O_3 and $\text{SiO}_2\text{-Al}_2\text{O}_3$ supports. If it is considered that the active sites on ReOx species are oxygen vacancy sites created by interaction of hydrogen with ReOx-support, according to kinetic model proposed recently by Leiva et al. [34], then ReOx have a higher possibility of vacancy formation on SiO_2 support during the initial stage of the reaction. This interpretation is supported by XPS results which

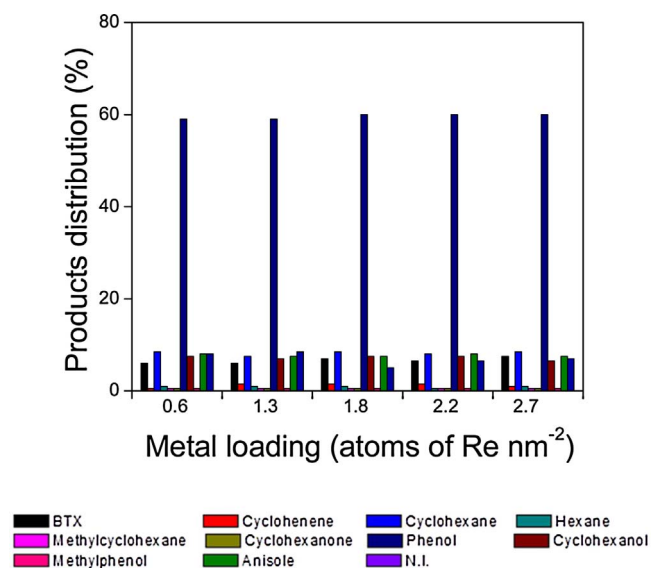


Fig. 12. Products distribution on ReOx(x)/SiO₂ catalysts calculated at 20% of guaiacol conversion.

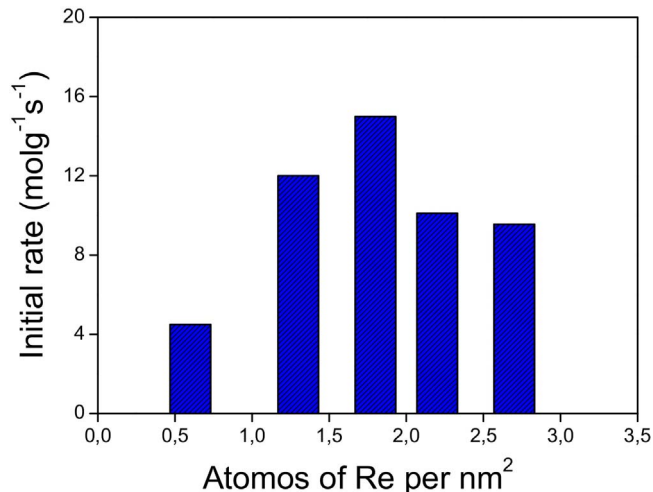


Fig. 13. Specific rates over ReOx(x)/SiO₂ catalysts.

show the presence of two ReOx species on the surface of the ReOx(1.8)/SiO₂ catalyst, while the other two catalysts contain one ReOx species. This suggests that the ReOx(1.8)/SiO₂ catalyst is more easily reducible, in agreement with TPR results, leading to an increase in the number of vacancy sites on this catalyst, and consequently the highest activity. In the case of ReOx(1.8)/SiO₂-Al₂O₃ and ReOx(1.8)/Al₂O₃ catalysts, in which one ReOx species was present, the higher activity of the former is attributed to its higher relative Re dispersion. Therefore, the data reveals that while the presence of oxygen vacancy sites is the dominant factor in the HDO of guaiacol over ReOx/supports catalysts, Re dispersion cannot be ignored when the catalysts exhibit similar reduction tendencies.

Fig. 11 shows the yield of products as a function of guaiacol conversion over ReOx(x)/SiO₂ catalysts. The main products on all the ReOx(x)/SiO₂ catalysts were phenol, BTX (mainly benzene and toluene and xylene in trace) and cyclohexane. Thus, these results follow the previously-described reaction network for guaiacol transformation in Fig. 8. The products distribution calculated at 20% of guaiacol conversion over the ReOx(x)/SiO₂ catalysts are shown in Fig. 12 and reveals nearly identical behavior over all the catalysts, indicating that the active sites present on these catalysts are similar. Furthermore, the formation of Re aggregates did not affect the products distribution.

The results of initial rate over ReOx(x)/SiO₂ catalysts are depicted in Fig. 13: the rate increases with increasing Re content up to 1.8 atoms of Re nm⁻², and then decreases. The initial linear increase of the rate of guaiacol conversion reflects an increase in the amount well-dispersed Re oxide species, resulting in an increase in the formation of oxygen vacancies (active sites). This is consistent with XPS results which showed an increase in Re dispersion up to a loading of 1.8 atoms of Re per nm² of support. Along the same line, the formation of Re aggregates as evidence by XPS, UV-vis-DR and Raman results led to decrease in the initial rate at higher loadings.

4. Conclusion

Re oxide catalysts supported on SiO₂, Al₂O₃ and SiO₂-Al₂O₃ were synthesized to study the support effect on catalytic activity and selectivity for the conversion of guaiacol (as a lignin model compound). The activity decreased in the order: SiO₂ > SiO₂-Al₂O₃ > Al₂O₃. TPR results showed that Re oxides are reduced at a lower temperature on SiO₂ support than over Al₂O₃ and SiO₂-Al₂O₃ supports, suggesting that the binding energy of Re-O-support on SiO₂ is lower, which translates to a more readily formation of oxygen vacancy sites (active sites associated with metal oxide defects created during course of the reaction). This interpretation is also supported by XPS results which showed the presence of two ReOx species on the SiO₂-supported catalyst, unlike the more difficult-to-reduce Al₂O₃ and SiO₂-Al₂O₃-supported catalysts in which only one ReOx species was observed. Meanwhile, the higher activity of the SiO₂-Al₂O₃-supported catalyst over Al₂O₃-supported catalyst is related to its higher Re dispersion as suggested by XPS results. For the effect of metal loading of ReOx(x)/SiO₂ catalysts, the activity trend correlates with Re dispersion obtained from XPS, whereby the highest catalytic activity was obtained with 1.8 atoms of Re per nm² of support (14% of Re) which exhibited the highest dispersion (formation of new active site). On the other hand, the loss of catalytic activity at higher rhenium contents is due to Re metal beginning to form aggregates, leading to loss of active sites in agreement with XPS, UV-vis-DR and Raman results.

Acknowledgments

The authors thank CONICYT-Chile for FONDECYT N° 1140528, PFB-27, ECOS-CONICYT N°C13E02, FONDECUID EQM 120096 grants and Red Doctoral REDOC.CTA, MINEDUC project UCO1202 at the University of Concepción. K. Leiva is indebted to CONICYT for doctoral grant.

References

- [1] Y. Nakagawa, Y. Shinmi, S. Koso, K. Tomishige, *J. Catal.* 272 (2010) 191–194.
- [2] S. Koso, Y. Nakagawa, K. Tomishige, *J. Catal.* 280 (2011) 221–229.
- [3] S. Koso, H. Watanabe, K. Okumura, Y. Nakagawa, K. Tomishige, *Appl. Catal B* 111–112 (2012) 27–37.
- [4] G. Busca, *Mater. Chem. Phys.* 19 (1988) 157–165.
- [5] M. Khurshid, M.A. Al-Daous, H. Hattori, S.S. Al-Khattaf, *Appl. Catal A* 362 (2009) 75–81.
- [6] M. Khurshid, S.S. Al-Khattaf, *Appl. Catal A* 368 (2009) 56–64.
- [7] Y. Amada, Y. Shinmi, S. Koso, T. Kubota, Y. Nakagawa, K. Tomishige, *Appl. Catal B* 105 (2011) 117–127.
- [8] S. Koso, N. Ueda, Y. Shinmi, K. Okumura, T. Kizuka, K. Tomishige, *J. Catal.* 267 (2009) 89–92.
- [9] D.E. Resasco, S. Crossley, *AIChE J.* 55 (2009) 1082–1089.
- [10] E. Laurent, B. Delmon, *Appl. Catal A* 109 (1994) 97–115.
- [11] P. Grange, E. Laurent, R. Maggi, A. Centeno, B. Delmon, *Catal. Today* 29 (1996) 297–301.
- [12] S.D. Robertson, B.D. McNicol, J.H. De Baas, S.C. Kloet, J.W. Jenkins, *J. Catal.* 37 (1975) 424–431.
- [13] C. Sepúlveda, R. García, P. Reyes, I.T. Ghampon, J.L.G. Fierro, D. Laurenti, M. Vrinat, N. Escalona, *Appl. Catal A* 475 (2014) 427–437.
- [14] K. Leiva, C. Sepúlveda, R. García, J.L.G. Fierro, N. Escalona, *Catal. Commun.* 53 (2014) 33–37.
- [15] V.N. Bui, D. Laurenti, P. Afanasiev, C. Geantet, *Appl. Catal B* 101 (2011) 239–245.
- [16] M. Ferrari, R. Maggi, B. Delmon, P. Grange, *J. Catal.* 198 (2001) 47–55.

- [17] C. Sepulveda, N. Escalona, R. Garcia, D. Laurenti, M. Vrinat, *Catal. Today* 195 (2012) 101–105.
- [18] I.T. Ghampson, C. Sepulveda, R. Garcia, L.R. Radovic, J.L.G. Fierro, W.J. DeSisto, N. Escalona, *Appl. Catal. A* 439–440 (2012) 111–124.
- [19] C. Ghampson, R. Sepulveda, J.L. Garcia, N. Garcia Fierro, W.J. Escalona, *Appl. Catal. A* 435–436 (2012) 51–60.
- [20] I.T. Ghampson, C. Sepulveda, R. Garcia, B.G. Frederick, M.C. Wheeler, N. Escalona, W.J. DeSisto, *Appl. Catal. A* 413–414 (2012) 78–84.
- [21] R.N. Olcese, M. Bettahar, D. Petitjean, B. Malaman, F. Giovannella, A. Dufour, *Appl. Catal. B* 115–116 (2012) 63–73.
- [22] I. Furikado, T. Miyazawa, S. Koso, A. Shimao, K. Kunimori, K. Tomishige, *Green Chem.* 9 (2007) 582–588.
- [23] Y. Shinmi, S. Koso, T. Kubota, Y. Nakagawa, K. Tomishige, *Appl. Catal. B* 94 (2010) 318–326.
- [24] A. Gutierrez, R.K. Kaila, M.L. Honkela, R. Slioor, A.O.I. Krause, *Catal. Today* 147 (2009) 239–246.
- [25] A. Shimao, S. Koso, N. Ueda, Y. Shinmi, I. Furikado, K. Tomishige, *Chem. Lett.* 38 (2009) 540–541.
- [26] M. Shetty, K. Murugappan, T. Prasomsri, W.H. Green, Y. Román-Leshkov, *J. Catal.* 331 (2015) 86–97.
- [27] N. Escalona, M. Vrinat, D. Laurenti, F.J. Gil Llambías, *Appl. Catal. A* 322 (2007) 113–120.
- [28] P.E. Ruiz, K. Leiva, R. Garcia, P. Reyes, J.L.G. Fierro, N. Escalona, *Appl. Catal. A* 384 (2010) 78–83.
- [29] G. Lagos, R. García, A.L. Agudo, M. Yates, J.L.G. Fierro, F.J. Gil-Llambías, N. Escalona, *Appl. Catal. A* 358 (2009) 26–31.
- [30] C. Sepulveda, V. Bellière, D. Laurenti, N. Escalona, R. Garcia, C. Geantet, M. Vrinat, *Appl. Catal. A* 393 (2011) 288–293.
- [31] C. Sepulveda, R. Garcia, N. Escalona, D. Laurenti, L. Massin, M. Vrinat, *Catal. Lett.* 141 (2011) 987–995.
- [32] K. Leiva, C. Sepulveda, R. Garcia, J.L.G. Fierro, G. Aguila, P. Baeza, M. Villarroel, N. Escalona, *Appl. Catal. A* 467 (2013) 568–574.
- [33] N. Escalona, J. Ojeda, R. Cid, G. Alves, A. López Agudo, J.L.G. Fierro, F.J.G. Llambías, *Appl. Catal. A* 234 (2002) 45–54.
- [34] K. Leiva, N. Martínez, C. Sepulveda, R. Garcia, C.A. Jiménez, D. Laurenti, M. Vrinat, C. Geantet, J.L.G. Fierro, I.T. Ghampson, N. Escalona, *Appl. Catal. A* 490 (2015) 71–79.
- [35] P. Arnoldy, E.M. van Oers, O.S.L. Bruinsma, V.H.J. de Beer, J.A. Moulijn, *J. Catal.* 93 (1985) 231–245.
- [36] B. Mitra, X. Gao, I.E. Wachs, A.M. Hirt, G. Deo, *Phys. Chem. Chem. Phys.* 3 (2001) 1144–1152.
- [37] R. Nava, B. Pawelec, P. Castaño, M.C. Álvarez-Galván, C.V. Loricera, J.L.G. Fierro, *Appl. Catal. B* 92 (2009) 154–167.
- [38] A. Naor, N. Eliaz, L. Burstein, E. Gileadi, *Electrochem. Solid State Lett.* 13 (2010) D91–D93.
- [39] W.T. Tysoe, F. Zaera, G.A. Somorjai, *Surf. Sci.* 200 (1988) 1–14.
- [40] L.L. Murrell, N.C. Dispenziere, R.T.K. Baker, J.J. Chludzinski, Strong metal-support, *Am. Interact. Chem. Soc.* (1986) 195–199.
- [41] J.M. Herrmann, Strong metal-support interactions, *Am. Interact. Chem. Soc.* (1986) 200–211.
- [42] M. Spichiger-Ulmann, A. Monnier, M. Koudelka, J. Augustynski, Strong metal-support interactions, *Am. Interact. Chem. Soc.* (1986) 212–227.
- [43] K. Fang, J. Ren, Y. Sun, *J. Mol. Catal. A: Chem.* 229 (2005) 51–58.
- [44] B. C. Peng, S. Zhao, S. Kasakov, Foraita, J.A. Lercher, *Chem. – A Eur. J.* 19 (2013) 4732–4741.
- [45] A.B. Dongil, I.T. Ghampson, R. Garcia, J.L.G. Fierro, N. Escalona, *RSC Adv.* 6 (2016) 2611–2623.
- [46] N. Koike, S. Hosokai, A. Takagaki, S. Nishimura, R. Kikuchi, K. Ebitani, Y. Suzuki, S.T. Oyama, *J. Catal.* 333 (2016) 115–126.
- [47] A. Cho, H. Kim, A. Iino, A. Takagaki, S. Ted Oyama, *J. Catal.* 318 (2014) 151–161.
- [48] S. Ted Oyama, H. Zhao, H.-J. Freund, K. Asakura, R. Włodarczyk, M. Sierka, *J. Catal.* 285 (2012) 1–5.
- [49] C. Cristiani, P. Forzatti, G. Busca, *J. Catal.* 116 (1989) 586–589.
- [50] E. Laurent, B. Delmon, *Appl. Catal. A* 109 (1994) 77–96.
- [51] V.N. Bui, D. Laurenti, P. Delichère, C. Geantet, *Appl. Catal. B* 101 (2011) 246–255.
- [52] T. Nimmanwudipong, R.C. Runnebaum, D.E. Block, B.C. Gates, *Energy Fuels* 25 (2011) 3417–3427.
- [53] Y. Yang, C. Ochoa-Hernández, V.A. de la Peña O’Shea, P. Pizarro, J.M. Coronado, D.P. Serrano, *Appl. Catal. B* 145 (2014) 91–100.